This is a repository copy of *High pressure CO2 CCS pipelines: Comparing dispersion models with multiple experimental datasets*.

White Rose Research Online URL for this paper:
http://eprints.whiterose.ac.uk/104231/

Version: Accepted Version

High pressure CO_2 CCS pipelines: Comparing dispersion models with multiple experimental datasets

Christopher J. Wareing[a,b,*], Michael Fairweather[a], Samuel A.E.G. Falle[c], Robert M. Woolley[a], Abigail M.E. Ward

[a]*School of Chemical and Process Engineering, University of Leeds, Leeds LS2 9JT, UK.*
[b]*School of Physics and Astronomy, University of Leeds, Leeds LS2 9JT, UK.*
[c]*School of Mathematics, University of Leeds, Leeds LS2 9JT, UK.*

Abstract

Carbon capture and storage (CCS) presents the short-term option for significantly reducing the amount of carbon dioxide (CO_2) released into the atmosphere from the combustion of fossil fuels, thereby mitigating the effects of climate change. Enabling CCS requires the development of capture, storage and transport methodologies. The safe transport of CO_2 in CCS scenarios can be achieved through pipelines or by shipping. Either way, transport and temporary storage of pressurised liquid CO_2 will be required and subject to quantitative risk assessment, which includes the consideration of the low-risk, low-probability puncture or rupture scenario of such a pipeline, ship or storage facility. In this work, we combine multiple experimental datasets all concerned with the atmospheric free release of pure and impure liquid CO_2 from CCS-transport-chain-relevant high pressure reservoirs and perform the first multiple dataset comparison to numerical models for both pure and im-

*Corresponding author. Tel: +44 113 343 3871. Fax: +44 113 343 5090
Email address: C.J.Wareing@leeds.ac.uk (Christopher J. Wareing)
URL: http://www.maths.leeds.ac.uk/~cjw (Christopher J. Wareing)

pure jets in dry ambient air with no water vapour. The results validate the numerical approach adopted and for the prediction of such releases, highlight the significance of the mixture fraction at the release point, over the mixture composition itself. A new method for impure CO_2 dispersion modelling is introduced and limited preliminary comparisons of impure CO_2 data and predictions are performed. No clear difference between pure and impure releases is found for the cases considered.

1. Introduction

Carbon capture and storage (CCS) refers to a set of technologies designed to reduce carbon dioxide (CO_2) emissions from large industrial point sources of emission, such as coal-fired power stations, in order to mitigate greenhouse gas production. The technology involves capturing CO_2 and then storing it in a reservoir, instead of allowing its release to the atmosphere, where it contributes to climate change. Once captured, the CO_2 is generally transported in a liquified state and stored, typically underground, or used for processes such as enhanced oil recovery.

The fluid dynamic modelling of liquid CO_2 poses a unique set of problems due to its unusual phase transition behaviour and physical properties. Liquid CO_2 has a density comparable with that of water, but has a viscosity of magnitude more frequently associated with gases. These properties make the transport of dense phase CO_2 an economically viable and attractive propo-

2

sition. However, due to it possessing a relatively high Joule-Thomson expansion coefficient, calculations and experimental evidence confirm that the rapid expansion of an accidental release reaches temperatures below 194 K. Due to this effect, solid CO_2 forms at temperatures below the triple point temperature (216.6 K) following a pipeline puncture or rupture, whether directly from liquid or via a vapour-phase transition. Additionally, CO_2 sublimes at ambient atmospheric conditions, which is a behaviour not seen in most other solids, and is an additional consideration when modelling flows such as these. Predicting the correct fluid phase during the discharge process in the near-field is of particular importance given the very different hazard profiles of CO_2 in the gas and solid states. The safe operation of CO_2 pipelines is of paramount importance then, as the inventory associated with a cross-country pipeline would likely be several thousand tonnes, and CO_2 has a toxic effect above 5% concentration and causes hyperventilation above 2% (Connolly and Cusco, 2007; Wilday et al., 2009).

The University of Leeds near-field CO_2 dispersion mathematical model (Wareing et al., 2013a), has been developed and validated for free releases of CO_2 into air for two data sets; the CO_2PipeHaz project (Woolley et al., 2013a,b) and the National Grid COOLTRANS project (Wareing et al., 2014a). It has also been validated against small-scale laboratory releases and dry ice particle behaviour (Wareing et al., 2013b, 2015a), punctures of buried pipelines (Wareing et al., 2014b) and ruptures of buried pipelines (Wareing et al., 2015b,c).

In this paper, we perform a comparison to a wider range of experimental data currently available regarding near-field liquid CO_2 dispersion. We

3

also introduce an impure equation of state and compare with new impure near-field CO_2 dispersion experimental data from multiple sources. In the next Section we reproduce the relevant background to this area. Following that in Section 3 we present the details of the experimental data sources. In Section 4 we briefly present details of our mathematical model and introduce the modifications for impure CO_2, including determination of a suitable equation of state. In Section 5 we describe the numerical methodology used herein. The comparison between data and predictions is discussed in Section 6. Finally, conclusions are presented in Section 7.

2. Background

In this section, we consider the growing number of recent publications that have examined the release and dispersion of CO_2, revisiting our review from Wareing et al. (2014a) that summarised the extensive review provided by Dixon et al. (2012) in the light of new and related additions to the literature.

MMI Engineering presented dispersion simulations (Dixon and Hasson, 2007) employing the ANSYS-CFX computational fluid dynamics (CFD) code. Solid CO_2 particles were simulated by a scalar representing the particle concentration, avoiding the overhead of full Lagrangian particle tracking. Dixon et al. (2012) note that this method assumed a constant particle diameter and temperature at the sublimation temperature of $194.25\,\mathrm{K}$ in order to calculate heat and mass exchange between the particles and the gas phase. Following this work up, Dixon et al. (2009) used a full Lagrangian particle tracking method, but still assumed particles to be at the sublimation temperature. Dixon et al. (2012) noted that since the rate of sublimation increases as par-

4

ticle size decreases, an improved distribution of the source of the CO_2 gas resulting from particle sublimation could be obtained by allowing for varying particle size and for the fact that temperature is expected to fall below the sublimation temperature in the near-field of a release.

Webber (2011) considered a methodology for extending existing two-phase homogeneous integral models for flashing jets to the three-phase case for CO_2. Webber noted that as the flow expands from the reservoir conditions to atmospheric pressure, temperature, density and the jet cross-sectional area would vary continuously through the triple point, whilst the mass and momentum would be conserved. This led to the conclusion that there must be a discontinuity in the enthalpy and CO_2 condensed phase fraction, in a similar manner to the energy change associated with passing through a hydraulic jump. In the development of our composite equation of state for modelling CO_2 near-field sonic dispersion (Wareing et al., 2013a), we confirmed this in a conservative shock capturing CFD code and highlighted the importance of fully accounting for the solid phase and latent heat of fusion; the near-field structure of the jet as well as the fraction of solid phase material is different when this is correctly accounted for.

Witlox et al. (2009, 2011) discussed the application of the software package PHAST to CO_2 release and dispersion modelling. Witlox et al. (2009) described an extension to the model in PHAST (v.6.53.1) to account for the effects of solid CO_2, including the latent heat of fusion. The modifications to the model consist principally of changing the way in which equilibrium conditions were calculated in the expansion of CO_2 to atmospheric pressure in order to ensure that below the triple point, conditions followed the sublima-

tion curve in the phase diagram, rather than extrapolating the evaporation curve (which diverges considerably from reality, hence the limitations of the Peng and Robinson (1976) and Span and Wagner (1996) equations of state to above the triple point only). In Witlox et al. (2011), the results of sensitivity tests were reported for both liquid and supercritical CO_2 releases from vessels and pipes calculated with the revised PHAST model. The public release of the CO2PIPETRANS datasets and associated industrial projects, e.g. (Ahmad et al., 2013), has validated the development of this approach, which we also adopted in part for our composite equation of state (Wareing et al., 2013a).

E.ON have published a number of studies (Mazzoldi et al., 2008a,b, 2011; Hill et al., 2011). Of these, the most relevant to this work are Mazzoldi et al. (2011) and Hill et al. (2011). These consider atmospheric dispersion from pipeline and vessel releases. The former paper compared simulations from the heavy gas model ALOHA to the CFD model Fluidyn-Panache. Only the gaseous stage of the release was modelled. In the second work (Hill et al., 2011), the authors presented CFD and PHAST simulations of dense-phase CO_2 releases from a 500mm diameter hole in a pipeline, located at an elevation of 5m above level ground. Steady-state flow rates were calculated at the orifice assuming saturated conditions. CFD simulations were performed using the ANSYS-CFX code with a Lagrangian particle tracking model for the solid CO_2 particles, with three size distributions: 10 to 50 micrometers, 50 to 100 micrometers and 50 to 150 micrometers. Simulations were also performed without particles. Their results showed that sublimation of the particles led to a cooling of the CO_2 plume, affecting dispersion behaviour,

6

although the results were relatively insensitive to particle size. Gas concentrations downwind from the release were reportedly somewhat lower using PHAST (v.6.6) as compared to the CFD results. No comparison to experiment was performed.

Dixon et al. (2012) note that in the Lagrangian model of Hill et al. (2011) their particle tracks followed closely the plume centreline, rather than being spread throughout the plume. Dixon et al. (2012) went on: turbulence will have the effect of bringing particles into contact with parts of the jet at a higher temperature and lower CO_2 concentration, thereby tending to increase the rate of sublimation and increase the radius of the region cooled by the subliming particles. In their work, Dixon et al. (2012) included turbulent dispersion effects in the CFX model. Further, they assumed that the solid particles are much smaller with an initial particle diameter of 5 micrometers. They made that choice based on an analysis of CO_2 experiments. In addition, this particle size distribution is supported by the model recently developed by Hulsbosch-Dam et al. (2012a,b), which suggested that the particle diameter would be around 5 micrometers for CO_2 releases at a pressure of $10\,\mathrm{MPa}$, when the difference between the CO_2 and ambient temperatures is around 80°C. They stated that the effect of having smaller particles in their model was likely to cause more rapid sublimation, which should produce a more significant reduction in gas temperature in the free jet. Recent examination of particle size distribution in releases of supercritical CO_2 from high pressure has shown that even smaller particles immediately post Mach shock are indeed the case (Liu et al., 2012b), on the order of a few micrometers, which we confirmed in laboratory releases from the liquid phase (Wareing et al.,

2013b).

Dixon et al. (2012) employ a Bernoulli method which they found "to provide reasonable predictions of the flow rate for the sub-cooled liquid CO_2 releases". Differences were apparent between the integral model and the CFD model results. The integral model predicted temperatures that they noted were too low in the near-field, and which then returned too rapidly to atmospheric levels (see Dixon et al. (2012) Figure 3.). The CFD model was noted to be in general better, although in the near-field ($< 10\,\mathrm{m}$ from the orifice) it was still not clear whether this was the case. Further, the CFD model appears to under-predict the spreading rate of the jet.

Liu et al. (2014) present simulations of free-jet CO_2 dispersion from high pressure pipelines using a non-ideal gas equation of state - specifically the Peng-Robinson (Peng and Robinson, 1976) equation. They obtained good agreement compared to the limited data available from the CO2PIPETRANS datasets (no data is available close to the shock-containing expansion region), but do not model the solid phase of CO_2 and hence are limited to predicting supercritical releases that do not cool below the triple point.

Wareing et al. (2013a) presented a composite equation of state for the modelling of high pressure liquid CO_2 releases that accounts for phase changes and the solid phase and went on to validate against venting releases from the CO_2PipeHaz project (Woolley et al., 2013a,b) and the COOLTRANS research programme (Wareing et al., 2014a). The model demonstrated good quantitative and qualitative agreement with the experimental data regarding temperature and concentration in the near- and far-field. More recently, we have applied the same model to punctures of a buried high pressure dense

phase pipeline (Wareing et al., 2015a) and a rupture of a buried 150 mm-diameter pipeline (Wareing et al., 2015b), at a quarter-scale of the full-scale pipelines intended in the UK White Rose CCS network (Cooper and Barnett, 2014). In both cases, the model shows reasonable agreement with the data, predicting jet temperatures, structures and behaviour, as well as predicting particle behaviour.

Woolley et al. (2014a) published a paper linking the elements of the CO_2PipeHaz project together, for the first time numerically modelling a complete chain rupture and consequent dispersion event in realistic topography. This included pipeline decompression linked to near-field sonic shock-capturing simulation of the flow from the pipe ends through the crater linked into the far-field, where constant source conditions on a plane above the crater were taken as input into FLACS and ANSYS-CFX simulations. These were taken as constant source conditions and the transient nature of the near-field decompression was not modelled. Gant et al. (2014) had previously considered the validation of FLACS and ANSYS-CFX in the far-field for this application, using predictions for the near-field from our composite model (Wareing et al., 2013a), albeit again modified for input into such commercial software. Wen et al. (2013) presented a number of far-field simulations of venting and horizontal above ground releases, with successful validation, also using predictions for the near-field from our composite model (Wareing et al., 2013a) for input conditions, but with less modification for input into their software.

In this paper, we return to near-field free dispersion releases above ground into dry air, and extend previous experimental data comparisons to all the

available data in the literature. We also present our extended numerical model for impure CO_2 and compare this to impure experimental data, as well as highlighting similarities and differences compared to pure predictions and data.

3. Sources of experimental data

3.1. CO2PIPETRANS

Phase 2 of the DNV-GL led CO2PIPETRANS[1] joint industry project (JIP) obtained a large amount of data from experiments designed to assist in the design of CO_2 pipelines and fill knowledge gaps that were identified during the execution of CO2PIPETRANS Phase 1, which resulted in the DNV GL recommended practice document DNV-RP-J202[2] entitled "Design and operation of CO_2 pipelines."

Relevant to the work herein, CO2PIPETRANS Phase 2 contained dense phase CO_2 release modelling validation data from two complimentary programmes of medium scale CO_2 release experiments conducted by DNV GL for BP (data set 1, hereafter DS1) and by DNV GL for Shell (data set 2, hereafter DS2). Further depressurisation tests on a CO_2 pipeline (data set 3) and experimental discharge data for large diameter CO_2 releases (data set 4) were carried out. Full details can be found in Brown et al. (2014a). DS1 consisted of tests 1-11 with a repeat of test 8. All were liquid phase

---

[1]https://www.dnvgl.com/oilgas/joint-industry-projects/ongoing-jips/co2pipetrans.html Accessed 2016-Aug-02.

[2]http://rules.dnvgl.com/docs/pdf/DNV/codes/docs/2010-04/RP-J202.pdf Accessed 2016-Aug-02.

releases. Test 1 did not record temperature data in the plume and we therefore exclude it. Tests 3 and 6 involved an extension tube and we therefore exclude them for the reason of not being free releases. Tests 4 and 7 involved an instrumented target and we therefore exclude them for the reason of not being free releases. Test 10 was pointed downwards into the ground and we therefore excluded it for not being a free release. Tests 8, its repeat test 8R and test 9 all considered releases without buffer pressure and therefore did not mimic large-scale pipeline, shipping or storage facilities and did not produce steady-state data. We therefore exclude them. Tests 2, 5 and 11 have been included here. From DS2, tests 3, 5 and 11 are the only suitable liquid phase releases that approximate steady state conditions. Again, all are pure CO_2 releases and all have been included here. The other tests are transient releases. Data sets 3 and 4 contain large diameter CO_2 releases where accurate measurements in the near-field close to the release were not possible. Hence no data from data sets 3 and 4 have been included in this comparison. We present the pertinent details of experimental data used in this work in Table 1. Complete details can be found in the reports accompanying the CO2PIPETRANS data releases.

3.2. COOLTRANS

National Grid initiated the 3-year TRANSportation of Liquid CO_2 research programme (COOLTRANS) (Cooper, 2012) at the end of 2010 in order to "address knowledge gaps relating to the safe design and operation of onshore pipelines for transporting dense-phase CO_2 from industrial emitters in the UK to storage sites offshore". This included developing the capability for modelling the low-probability, high-impact worst case - an accidental re-

11

lease from a buried pipeline that contains CO_2 in the dense-phase. Learning from these studies was subsequently combined with a range of other information to develop an appropriate quantified risk assessment (QRA) for a dense-phase CO_2 pipeline. The programme included theoretical studies by University College London (UCL), the University of Leeds and the University of Warwick, carried out in parallel to provide high-fidelity numerical models for the pipeline outflow (UCL), near-field dispersion behaviour (University of Leeds) and far-field dispersion (University of Warwick) behaviour associated with below-ground CO_2 pipelines that are ruptured or punctured. Experimental work and studies using currently available practical models for risk assessment were carried out by DNV GL (Allason et al., 2012). Full details of the experimental data used herein from this project can be found in Wareing et al. (2014a). We present the pertinent details of experimental data used in this work in Table 2.

3.3. $CO_2PipeHaz$

The EU FP7-funded CO_2PipeHaz (2010-2013) project "addressed the fundamentally important and urgent issue regarding the accurate predictions of fluid phase, discharge rate, emergency isolation and subsequent atmospheric dispersion during accidental releases from pressurised CO_2 pipelines to be employed as an integral part of a large scale carbon capture and storage chain"[3]. More details of the project can be found in Woolley et al. (2014b). Details of the experimental data used herein from CO_2PipeHaz can be found in Woolley et al. (2012, 2013a) for Tests 6, 7 and 8, and in Woolley et al.

---

[3]http://www.co2pipehaz.eu/overview.htm Accessed 2016-Aug-02.

(2013b) for Tests 11, 12 and 13, all concerning releases from a liquid phase pure CO_2 reservoir. We present the pertinent details of experimental data used in this work in Table 3, reproduced from Woolley et al. (2012, 2013a,b).

3.4. HSL data set

In Pursell (2012) data are presented from laboratory-scale CO_2 release experiments. Measurements were taken of the outflow and near-field dispersion behaviour in an expanding CO_2 jet, from both liquid and gaseous phase reservoirs. For this work, we consider two tests: HSL Test C and HSL Test D, both from a pure CO_2 liquid phase reservoir. Compared to the other data sets used in this comparison, it is notable that these measurements are taken on a smaller scale using 2.0 mm and 4.0 mm diameter nozzles. We present the pertinent details of experimental data used in this work in Table 4.

3.5. CO_2QUEST

Following on from CO_2PipeHaz, the most recent CO_2 dispersion data comes from the EU FP7-funded CO_2QUEST project (2013-2016) that involves "the collaboration of 12 industrial and academic partners in Europe, China and Canada and focusses on the development of state-of-the-art mathematical models along with the use of large scale experiments to identify the important CO_2 mixtures that have the most profound impact on the different parts of the CCS chain"[4]. A more complete description of the CO_2QUEST project can be found in Brown et al. (2014b). In this work, we take experimental data from a number of pure and impure releases performed by

---

[4]http://www.co2quest.eu/index.php Accessed 2016-Aug-02.

INERIS in France (Proust, Hebrard and Jamois, 2016) and DUT in China (Chen et al., 2016). Specifically, INERIS tests QUEST T12 and QUEST T14 concern near-field measurements of pure CO_2 releases. INERIS tests QUEST T9, T13, T15, T16, T19 and T22-T25 all concern comparable releases of impure CO_2 and were designed to be directly comparable to the pure test results, in order to elucidate any differences introduced by CO_2 impurities. Both DUT tests concern pure CO_2, but are on the largest scale that we are aware of that measure near-field conditions relevant to this work. We present the pertinent details of experimental data used in Table 5.

4. Mathematical model and numerical method

The mathematical model and numerical approach is essentially the same as that adopted and validated in our earlier papers. Complete details of this model can be found in Wareing et al. (2013a). This model has previously been validated in the literature in separate works against the COOLTRANS data (Wareing et al., 2014a), Tests 6, 7 and 8 of the CO2PIPEHAZ data (Woolley et al., 2012, 2013a) and the remaining CO2PIPEHAZ data (Tests 11, 12 and 13) in a conference paper (Woolley et al., 2013b). In this paper, the validation is extended from those 7 tests, to three further independent datasets - CO2PIPETRANS, HSL and CO2QUEST - that contain 17 further suitable pure CO_2 tests. Therefore we are able to investigate the validity of the model and the consistency of the experimental data in a much larger number of pure CO_2 tests. Here, as we are also extending this model to consider impure CO_2 dispersion, we summarise details of our original composite equation of state (EoS) for pure CO_2 and present the implementation

of an impure CO_2 EoS in our model. The nature of the new extension is in the inclusion of complex new equations of state and associated changes to the homogeneous model, detailed below. The extended number of datasets introduce 9 new impure CO_2 tests against which we can validate the new impure CO_2 dispersion model.

4.1. Equation of state for pure CO_2

Our composite EoS, as described in Wareing et al. (2013a) predicts the thermophysical properties of the three phases of CO_2 for the range of temperatures of relevance to CO_2 dispersion from releases at sonic velocities i.e. those of interest to the CCS industry. This EoS is designed to be convenient for computational fluid dynamic applications; the gas phase is determined from the Peng-Robinson EoS (Peng and Robinson, 1976), and the liquid and condensed phases from tabulated data generated with the Span and Wagner EoS (Span and Wagner, 1996). Previously, we modelled the solid phase using the DIPPR® Project 801 database [5], academic access to which can be gained through the Knovel library [6]. We now use the Jäger and Span EoS (Jäger and Span, 2012) for solid CO_2. Air is modelled by an ideal gas equation of state with $\gamma_a = 7/5$.

4.2. Impure CO_2

Very few forms of EoS are available for the range of pressure and temperature in these near-field simulations. Specifically, we are aware of two in the literature that have been validated that include the necessary solid

---

[5]http://www.aiche.org/dippr/ Accessed 2016-Aug-02.
[6]http://why.knovel.com Accessed 2016-Aug-02.

phase - EOS-CG (Gernert and Span, 2016) embedded in the TREND software (Span et al., 2015), and PC-SAFT (see Diamantonis et al., 2013, and references therein) embedded in the Physical Properties Library (PPL). Others are limited to pipeline pressures and temperatures (e.g. Demetraides and Graham, 2016) and/or do not model the solid phase - e.g. most cubic EoS, see the comparisons of Diamantonis et al. (2013) and those in the thesis of Li (Li, 2008) for more details. Here we examine TREND version 2.0 (obtained by private communication, August 2015) and PPL as developed in CO2QUEST for impure CO_2 (obtained through the CO2QUEST collaboration, September 2015). For both, we assume a mixture of 96% CO_2 and 4% N_2, typical of the type of and maximum level of impurity expected in UK CCS pipelines Cooper and Barnett (2014). It should be noted that this is not a mature research area: both TREND and PPL are still in development. Both currently use the Jäger and Span (2012) EoS in the solid phase and assume no solubility of impurity in the solid phase.

As neither EoS has been demonstrated to work in the near-field for an impure CO_2 release, we first looked at simple decompression from high pressure CO_2 to low pressure, both with and without a heat source. The inclusion of a heat source partially mimics the mixing with ambient air that occurs during the release. This is described by

$$dU = -PdV - \kappa(T - T_a), \tag{1}$$

where $U(P,T)$ is the internal energy per unit mass, P is the pressure, $V(P,T)$ is the specific volume, T is the temperature, T_a the (constant) ambient temperature and κ a constant that determines the amount of heating.
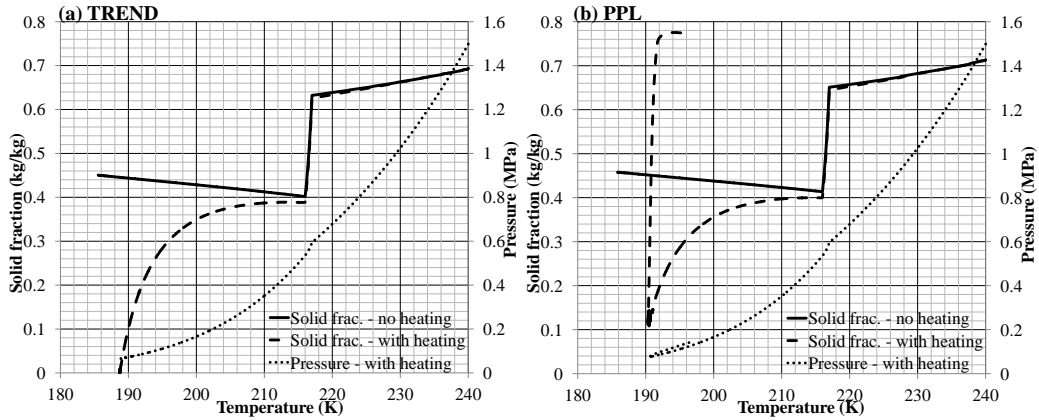
16

Figure 1: Condensed phase CO_2 and pressure in a decompression computed with TREND in (a) and computed with PPL in (b). Solid lines: solid fraction during isentropic decompression ($\kappa = 0$). Dashed lines: solid fraction during decompression with heating ($\kappa = 1$). Dotted lines: pressure during decompression with heating ($\kappa = 1$).

As can be seen comparing TREND in Figure 1(a) to PPL in Figure 1(b), there is little difference for the isentropic expansion (solid lines). However, when a heat source is added, TREND produces a smooth evaporation of solid CO_2 (dashed line in Figure 1(a)), but with PPL the solid mass fraction increases rapidly as atmospheric pressure is reached (shown in Figure 1(b)). Further investigation has revealed this is because there is a discontinuity at the dew line at low temperatures with PPL, making this version of PPL unsuitable for the current dispersion simulations. TREND is used for impure CO_2 modelling for the rest of this work. As noted, however, these EoS are undergoing further development with the intention that both should be applicable to the types of release of interest in CO_2 pipeline risk assessments, and for a wide range of impurities.

17

4.3. Homogeneous model

In previous work on dense-phase CO_2 releases from small nozzles and punctures (Wareing et al., 2014a,b), particles of solid CO_2 do not reach equilibrium with the CO_2 gas flow in the initial expansion due to the short distance between release point and Mach shock when compared to particle thermal and dynamic relaxation times and velocities (Wareing et al., 2013b). We therefore used a homogeneous relaxation model to take this into account. Since the EoS with impurities is only available for equilibrium, we use a very small relaxation time for pure CO_2 so that it is very close to equilibrium. The homogeneous relaxation model is described in Wareing et al. (2013a)

Modifications required for impure CO_2 are as follows. TREND can be used to determine the thermophysical properties of impure CO_2 as functions of pressure, P, and temperature, T. Since the properties vary rapidly near the dew line, we use a scaled pressure variable, x, defined by

$$
\begin{aligned}
x &= 1 + \log\left[e^{(1-y)} + \sqrt{\left\{e^{2(1-y)} - 1\right\}}\right] & y \leq 1, \\
x &= 1 + \log\left[e^{(1-y)} - \sqrt{\left\{e^{2(1-y)} - 1\right\}}\right] & y > 1,
\end{aligned}
\tag{2}
$$

where

$$
y = P/P_d(T),
\tag{3}
$$

and $P_d(T)$ is the pressure at the dew line. This ensures that x varies rapidly with P near the dew line and linearly elsewhere. Equation (2) can readily be inverted to give

$$
\begin{aligned}
y &= 1 - \log\left[\cosh(x-1)\right] & x \leq 1, \\
&= 1 + \log\left[\cosh(x-1)\right] & x > 1.
\end{aligned}
\tag{4}
$$

18

Given a table in terms of (x, T), it is simple to generate a table in terms of (ρ, T).

A conservative hydrodynamic code works in terms of the total density, ρ, and total internal energy per unit mass, U, so it is necessary to obtain the pressure and other quantities given ρ and U. Let α be the mass fraction of the CO_2 that is in the condensed phase and β be the mass fraction of CO_2 in a CO_2 - air mixture. The temperature is found by solving

$$U = \beta U_{CO_2}(\beta\rho, T) + (1 - \beta)U_{air}(T), \tag{5}$$

where U_{CO_2} and U_{air} are the internal energies for CO_2 and air. The pressure is then given by

$$P = (1 - \beta)\frac{RT\rho}{[m_a(1 - \alpha\beta\rho/\rho_c)]} + P_{CO_2}(\beta\rho, T), \tag{6}$$

where $\rho_c(\beta\rho, T)$ is the density of condensed phase CO_2, m_a is the molecular mass of air and $\alpha = \alpha(\beta\rho, T)$.

This assumes that the CO_2 - air mixture behaves as if the CO_2 has density $\beta\rho$ and temperature T. This is obviously not true at high pressures where the behaviour of the gaseous phase departs from the ideal gas equation of state. Fortunately, the mixing between CO_2 and air occurs at atmospheric pressure and temperatures significantly below the triple point. In this regime the gaseous phase does obey the ideal equation of state and one can also neglect the solubility of nitrogen and oxygen in solid CO_2 (as TREND does).

4.4. Implementation

Both equations of state are implemented via look-up tables in MG, an adaptive mesh refinement (AMR) RANS hydrodynamic code (Falle, 1991). The code employs an upwind, conservative shock-capturing scheme and is able to employ multiple processors through parallelisation with the message passing interface (MPI) library. Integration in time proceeds according to a second-order accurate upwind scheme with a Harten Lax van-Leer (van Leer, 1977; Harten et al., 1983) (HLL) Riemann solver to aid the implementation of complex EoS. The code also uses AMR (Falle, 2005), which reduces the memory and computation time by an order of magnitude. Further details can be found in Wareing et al. (2013a) and in the references above.

5. Numerical methodology

In computationally simulating the releases considered below, we employed the same methodology as Wareing et al. (2013b), solving Favre-averaged, density-weighted forms of the transport equations for mass, momentum, total energy (internal energy plus kinetic energy) and scalar transport, closed using a compressibility-corrected version of the $k - \epsilon$ turbulence model. We used a two-dimensional cylindrical polar axisymmetric coordinate system. Numerical simulations were performed employing the inlet conditions listed in Table 6 as input conditions in the region defined by $r < 0.5\,D$ (dimensions are scaled by the vent exit diameter, D) on the $z = 0$ boundary. The initial state of the fluid in the domain consists entirely of stationary air at a pressure and temperature given in Table 6. Conditions in air are calculated via an ideal gas equation of state with $\gamma_a = 7/5$. The $r = 0$ axis was treated

as symmetric and the other r boundary as free flow, introducing air with the initial atmospheric condition if an in-flow was detected. This neglects the effects of a cross-flow in the atmosphere, but this is a reasonable approximation to make over the near-field range, where the momentum from the release is expected to dominate, and is supported by previous work (Wareing et al., 2013b; Woolley et al., 2013a). The $z = 0$ axis was fixed by the input conditions for $r < 0.5\,D$ and as a solid wall outside this region, ignoring any ability of the release to entrain air from behind the inlet for the purposes of this work. The other z axis was free-flow, again only allowing the in-flow of air with the initial atmospheric condition if in-flow was detected, for example as a result of vortices formed before the jet reaches steady state. Given that vortex structures may be present in the jet as it reaches steady state, velocities that lead to inflow can occur at the free-flow boundaries. Hence the boundary conditions are adjusted to ensure that only ambient air can flow into the domain, with the same properties as the initial condition, and no CO_2.

For the purposes of comparison to experimental data, we show predictions extracted from five numerical simulations in later figures. The inlet conditions for these simulations are shown in Table 6 and are enforced on every step at the $z = 0$ boundary for $r < 0.5\,D$. The first three inlet conditions have the same pressure and temperature and only vary liquid fraction at the nozzle to demonstrate the importance of this key parameter. They are based on COOLTRANS T7 and we refer the interested reader to Wareing et al. (2014a) for full details of these inlet conditions. The fourth set of inlet conditions are matched to QUEST T12 concerning a release of pure CO_2 in

the CO2QUEST project. The fifth set of inlet conditions idealise the fourth set of conditions for a mixture of 96% CO_2 and 4% N_2, typical of impurity levels expected in pipeline transport of CO_2 from power generation (Cooper and Barnett, 2014; Porter et al., 2015). Specifically, they achieve the same mass-flow rate and hence are directly comparable to the fourth set of inlet conditions and also the impure CO_2 tests from CO2QUEST. Both the fourth and fifth sets of inlet conditions were obtained from UCL as part of the CO2QUEST project. We have chosen to idealise the fifth set of inlet conditions in this way in order to explore whether there is a difference between pure and impure dispersion predictions that otherwise keep the dominating release factor - mass-flow - the same. There is no such pair of experiments in the CO2QUEST dataset. Pure Test 12 and impure Tests 14 and 15 are all similar. In the case of Test 14, the impurity and level of impurity is very similar to Test 12, but the pressure and temperature are different and hence mass flow rate is different. In the case of Test 15, the pressure and temperature are similar to the idealised case, but the impurities are different, even if the total level is very similar. If we had chosen for the fifth set of inlet conditions to model, e.g. Test 14, the mass-flow rate would have been different and hence the Mach shock would have been in a different location. This is a valid thing to do, but outside the scope of this work as we note in our conclusions.

6. Model comparisons with data

In the following figures we show comparisons of data and dispersion predictions. The plotted data points indicate experimental measurements of the

temperature in the dispersion plume at that location and are the simple average for that particular sensor during the steady state period. The experimental data during the steady state period has a variance on each measurement during the relevant time period of a degree or two. The temperature sensors used are typically accurate over the observed range to within $\pm 5\,K$ at worst, hence throughout all the plots shown the experimental data points should be assumed to have $\pm 5\,K$ error bars, although for clarity these error bars have not been plotted in the figures. The response time of the sensors is less than a second in all cases and hence less than the steady state period, which is at a minimum of 3 seconds, up to tens of seconds for some of the small diameter, large reservoir releases. Predictions shown are taken from steady state 2D axisymmetric simulations for the various inlet conditions noted in the figures, the full details of which were presented in the previous section and examples of which can be seen in Wareing et al. (2013a,b)

In Figure 2 we compare centreline temperature predictions with varying liquid fraction at the release point to centreline experimental temperature data. The first thing to note is that the experimental data is coincident within the $\pm 5\,K$ error up to $100\,D$, at temperatures around $190\,K$. After $100\,D$, the different experimental datasets diverge, each warming towards ambient conditions at a different rate. Scaling the centreline distance in nozzle diameters has created a nozzle-diameter-independent plotting of the experimental data. The predictions of temperature drop very rapidly through the Mach shock, which in this figure is at $\sim 8\,D$, so is visible by the drop to $166\,K$ pre-shock and then the rise to $194.25\,K$ post-shock. For the first $100\,D$ the predictions are slightly warm compared to the data. The pure CO_2 predictions
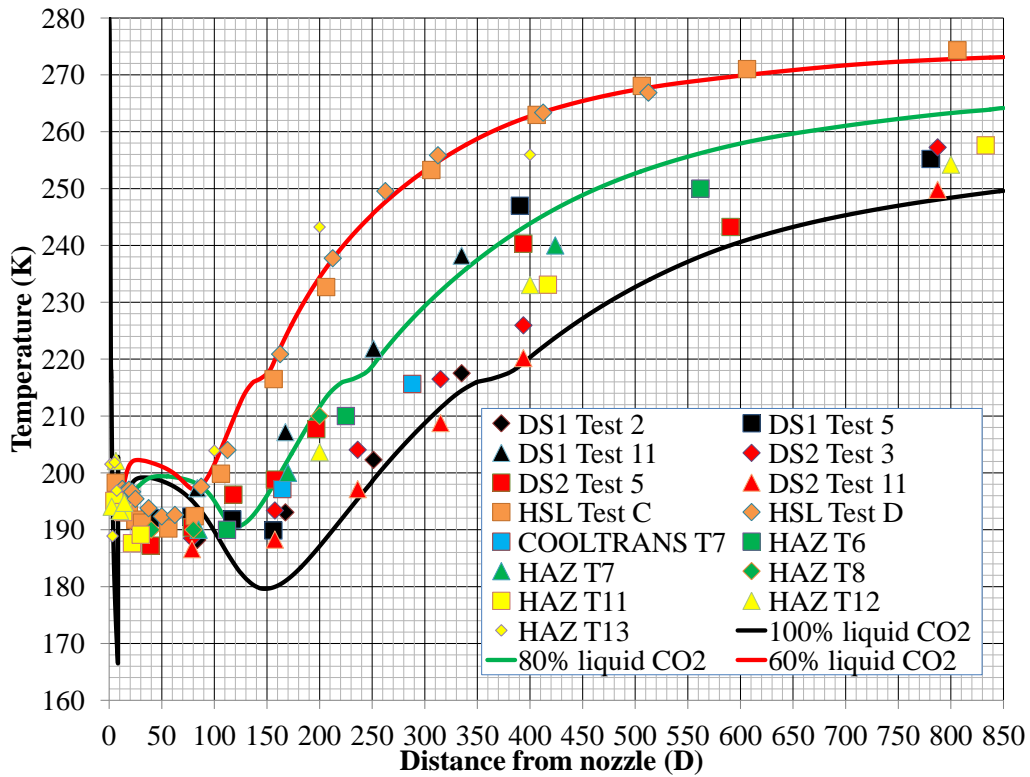
Figure 2: Experimental data (points) versus predictions (lines) of temperature along the centreline of an expanding liquid CO_2 jet release through a nozzle/vent/puncture from/in a high pressure reservoir. Multiple datasets are identified in the legend and every datapoint should be assumed to have a $\pm 5\,\mathrm{K}$ error, not shown in the figure. Predictions are shown based on the COOLTRANS T7 inlet conditions for 60%, 80% and 100% liquid fraction at the nozzle (see Table 6).

shown here employ the homogeneous relaxation model in the same way as used in Wareing et al. (2013b), which allows the gas temperature to vary compared to the solid temperature beyond the Mach shock. An equilibrium model would necessarily have a temperature of $194.25\,\mathrm{K}$ immediately after the Mach shock as this is the sublimation temperature at which gas and solid co-exist at atmospheric pressure. Evaporation of the solid then cools the flow along the centreline, as noted by us and other authors (see Section 2 for a discussion of this effect). Within error, the experimental data satisfyingly falls between these two extremes. The smallest nozzle diameter experiments (HSL Tests C and D) are the warmest at this point, which is to be expected as the solid particles are the furthest from equilibrium due to the proximity of the shock to the release point.

Further than $100\,\mathrm{D}$ along the centreline, the 100% liquid fraction prediction clearly remains the coldest of the three predictions into the far-field, bracketing the coldest extreme of the data at specific centreline distances, typically CO2PIPETRANS DS2 Test 11. This suggests that DS2 Test 11 was very close to 100% liquid at the release point. At the warm extremes of the data going into the far-field are HSL Tests C and D. These are captured by the 60% liquid prediction, although inferred rates in Table 4 are higher than that. This discrepancy could be related to the true liquid fraction at the nozzle or the fact that these tests are somewhat different to the other tests shown here, as they are the smallest diameter nozzles and were also performed in controlled laboratory conditions rather than outdoors. We have also shown in previous work that the choice of turbulence model in the numerical prediction affects the plume temperature into the far-field. Here

we have used a compressibility corrected $k - \epsilon$ model described in detail in Wareing et al. (2013a). So far, we have found this model provides the best fit to averaged CO_2 temperature dispersion data. Further work considering the unsteady jets produced by Reynolds-stress turbulence models will investigate this further. The 80% liquid prediction falls half-way between the 60% and 100% liquid predictions, suggesting that DS1 Test 11 may have had a liquid fraction at the nozzle around 80%. The variation in experimental data, though all are releases from high pressure (close to) 100% liquid reservoirs, can therefore be explained by variation of the liquid fraction at the release point, as differences in the experimental apparatus range from direct release from the reservoir, to release along elongated narrow-diameter pipes.

In Figure 3, we show radial comparisons of data and prediction at $80\,\mathrm{D}$, $\sim100\,\mathrm{D}$, $165\,\mathrm{D}$ and $400\,\mathrm{D}$ along the centreline of the jet. Whilst we show as many datasets as possible, here we only show the prediction for 100% liquid CO_2, which as might be expected brackets the lower temperature extreme of the data. Agreement between the multiple datasets across the wide range of centreline locations is clear from the figures, as well as a good fit by the predicted temperature in the dispersion plume. The advantage of this comparison is that it is now possible to clearly identify experimental data which is not comparable to the majority. The temperature of $210\,\mathrm{K}$ in the case of COOLTRANS T7 at z=$165\,\mathrm{D}$ and r=$32\,\mathrm{D}$ appears to be an outlier compared to the other measurements, both from that test and others. The identification of such points should simplify future experimental and model validation work.

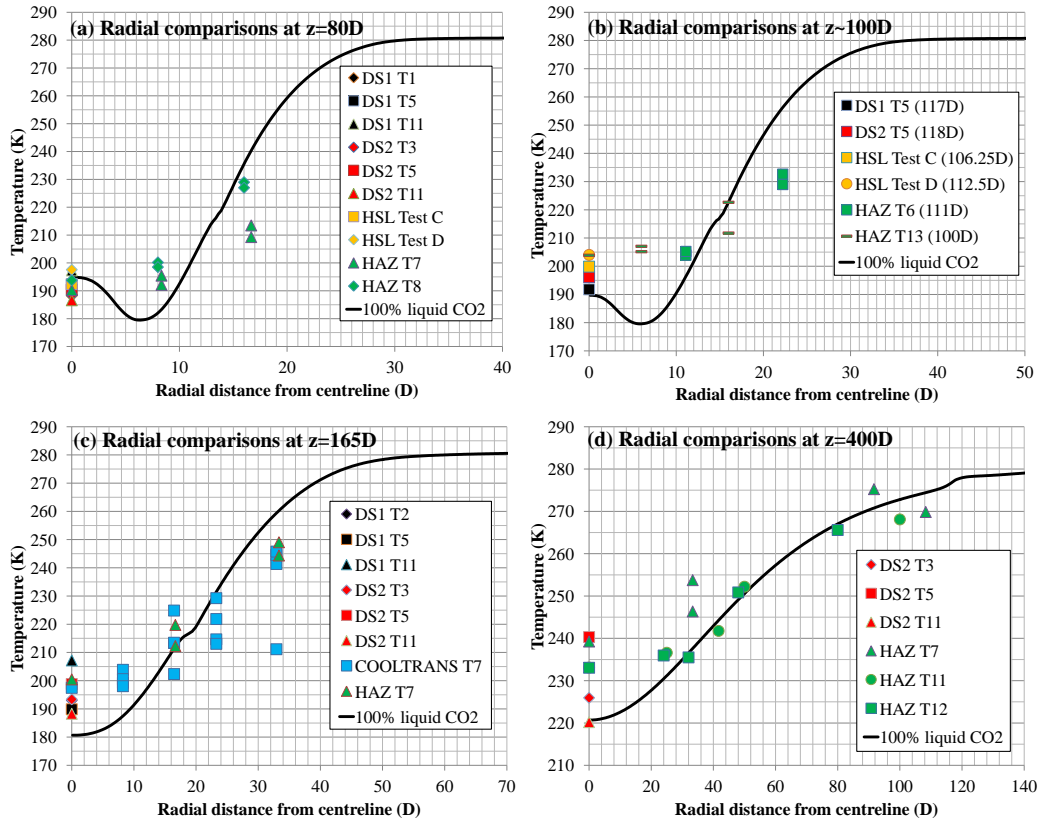Figure 4 shows a near-field comparison for both pure CO_2 releases (in

Figure 3: Experimental data (points) versus predictions (lines) for radial temperature distributions at various locations along the centreline of an expanding liquid CO_2 jet release through a nozzle/vent/puncture from/in a high pressure reservoir. Multiple datasets are identified in the legends and every data point should be assumed to have a $\pm 5\,\mathrm{K}$ error, not shown in the figures. Predictions are shown based on the COOLTRANS T7 inlet conditions for 100% liquid fraction at the nozzle (see Table 6).
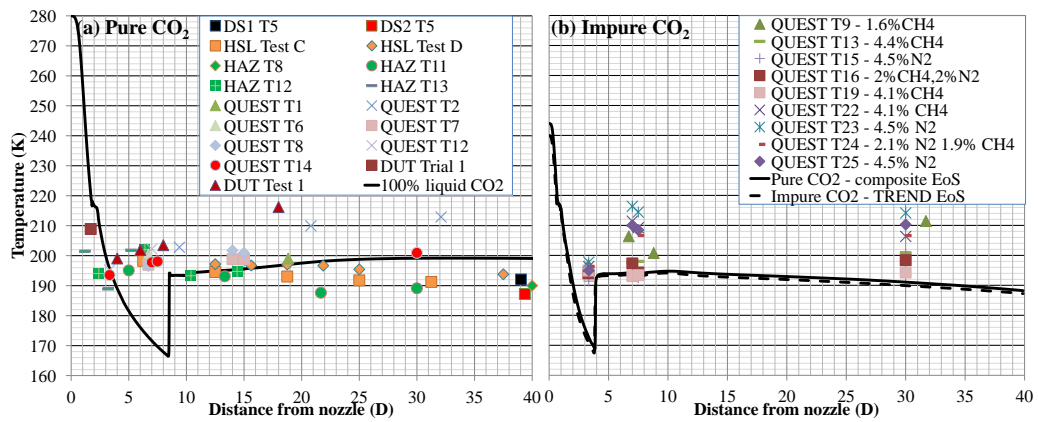
Figure 4: Experimental centreline near-field temperature data (points) for (a) pure and (b) impure releases of CO_2 from a high pressure reservoir. Multiple datasets are identified in the legends and every data point should be assumed to have a $\pm 5\,\text{K}$ error, not shown in the figures. Shown also are predictions of the temperature (lines) based on the COOLTRANS T7 inlet conditions for 100% liquid fraction in (a) and based on the pure and impure CO_2 inlet conditions in (b), matching reservoir conditions in QUEST T12 (see Table 6).

(a)) and impure CO_2 releases (in (b)). Near-field data and predictions up to $40\,D$ from the release point are shown for both cases. In the pure CO_2 case, data from all five sources is shown to be remarkably consistent, apart from the largest field-scale DUT tests, which given the release diameters of $50\,mm$ and $233\,mm$ are large-flow rate releases at the limit of near-field measurement capability. Larger scale experiments have been performed, but with limited near-field measurements using different methods; the numerical model used has been shown to be able to predict such experiments (Wareing et al., 2014a, 2015a,b). Within the Mach shock structure ($z < 8\,D$), experiment and prediction do not agree well, although the data shows some indication of upward trending temperature close to the release point. Given the rapid variation of pressure from tens of atmospheres to fractions of a percent of atmospheric just before the Mach shock, the rapid expansion and decrease in density and the large acceleration from typically $100\,\mathrm{m\,s^{-1}}$ at the nozzle to typically $400\,\mathrm{m\,s^{-1}}$ at the shock, it is perhaps not surprising that thermocouples designed to measure steady-state flows at atmospheric pressure struggle to capture the extreme gradients in the expanding jet. Beyond the Mach shock, temperatures around the sublimation temperature of $194.25\,K$ at atmospheric pressure are again seen. The spread of the data is in good agreement with this, bar the large-scale DUT Test 1 which has already been discussed and QUEST T2 which would seem to possess a warming trend suggestive of low liquid fraction. For future modelling, most of the datasets would appear to be close to equilibrium, behaving in the way expected from previous insights - the temperatures post-Mach-shock slowly drop from the sublimation temperature until all the solid has evaporated and then the dis-

persion plume begins to warm. The point at which this occurs is not shown in this figure and varies with liquid fraction at the nozzle, but can be seen in Figure 2.

Turning now to releases of impure CO_2 as shown in Figure 4b, multiple impure experimental datasets and two predictions are shown for comparative purposes. QUEST Tests 12, 13, 14, 15 and 16 were designed to be directly comparable for the purposes of differentiating the effects of impurities. The datasets are remarkably consistent but it should be noted that they are entirely sourced from INERIS through CO2QUEST. The closest near-field temperature measurements for small-scale releases have been obtained and all seem to agree on $194.25\,\mathrm{K}$. The predictions, which model QUEST T12 and its impure idealisation, would indicate the measuring point is very close to the Mach shock. The pure prediction (solid black line) models the release conditions from QUEST T12. The impure prediction is idealised to match the same release temperature and mass-flow as QUEST T12 (for the reasons set out in Section 5), and so is reasonably comparable to QUEST T15 with 4.5% N_2 for the level of impurity and QUEST T16 for the pressure and temperature and hence mass-flow. Perhaps not surprisingly for matched mass-flow, the two predictions are very similar - the low-level of impurity has very little effect and the position of the Mach shock is dominated by the initial pressure and mass flow rate. The recorded dispersion temperatures are very similar to that in pure CO_2 experiments and show no clear difference between type of impurity and total amount of impurity. Near-field temperature measurements of the dispersing plume alone clearly cannot differentiate between pure and impure CO_2 in this case. This is supported by the close

similarity of pure and impure predictions - the experimental accuracy of $\pm 5K$ is far greater than the difference between the predictions. This data would be hard pushed to differentiate between pure and impure releases in the near-field on that basis. We would like to reassure the reader that the EoS data used in this work does pick up a difference between pure and impure predictions - the presence of a two-phase region between the bubble and dew lines in the tabulated impure EoS data confirms this. Further experiments with different experimental setups are required to investigate differences between pure and impure CO_2 releases, at least for these levels of impurity. For example, the impure data shown here indicates a difference between the QUEST datasets T9 to T19 and T22-T25. Beyond the Mach shock, T22-T25 are characteristically warmer than the other tests. These are larger diameter tests, but in the middle of the range of nozzle sizes shown in previous figures, so it is not clear why they should be characteristically warmer than the other QUEST tests. Further work is required here to elucidate the reasons for these experimental differences, including experiments designed to show differences between pure and impure that are greater than the experimental accuracy. Through this work, future modelling efforts should now be able to refine their experimental validation procedures.

7. Conclusions

In this work we have performed the first multiple-dataset comparison between experimental data and numerical predictions for the dispersion of high pressure liquid CO_2 from CCS transport pipeline scenarios into dry air, extending previous validation from 7 tests to a total of 24 tests. A simple

31

non-dimensionalisation of experimental data according to nozzle diameter used here has provided the means to compare these multiple datasets from different projects and experimental procedures. It has revealed remarkable consistency between the experimental datasets. Predictions compare well to the experimental data and highlight the fact that liquid fraction reducing mass flow rate at the release point is of key importance in modelling CO_2 dispersion. It is our hope that the presentation of data from multiple sources in this extended validation highlights the differences between experimental tests and will aid researchers looking to validate dispersion models in the future.

Turning to impure CO_2, for the limited range of low-level impurity considered here, no clear difference to pure CO_2 releases is discernible in temperature dispersion data. This is reflected by the close agreement between pure and impure predictions of temperature in the dispersion plume. Differences between experimental datasets are noted. The publication of this work in the literature should allow future modelling work to account for these differences in their validation procedures. Further experimental work is required to discern any differences between such pure and impure CO_2 dispersion. It is worth noting that we chose numerical inlet conditions for the pure and impure cases in order to match mass-flow and explore whether an impurity level of 4% N_2 made any difference to the numerical predictions, as this was one aim of CO2QUEST. Real-life pipelines and transport facilities are likely to set pressure and temperature specifications. An impurity will therefore alter the density of the mixture and hence the mass-flow through a given orifice. Further exploration of such differences between transport-facility conditions

is required to quantify the effects of impurities further.

The numerical prediction of impure CO_2 dispersion requires complex equations of state. The use of TREND here has shown there is little difference between pure and impure temperature predictions for low-levels of impurity (4% N_2), but further work is required as the necessary impure equations of state are still under development and the available experimental data for validation is limited.

We have not considered the presence of water vapour in the air. The region in which water vapour will make a difference in the near-field is limited - the predictions have shown that no air mixes into the centre of the jet until approximately 40 release diameters downstream from the release point. Water vapour cannot affect this part of the jet, which includes the near-field Mach shock. The centreline predictions shown herein will be unchanged. Where water vapour in the air does become important is on the edges of the jet. Water droplets will condense once the temperature is below the dew point - this chiefly defines the visible extent of the jet. Further into the mixing region, at lower temperatures, water ice will form. Since water has a latent heat of fusion approximately five times greater than that of CO_2, it will act as an energy sink causing the CO_2 jet to be less cold (on the order of a few degrees at most in the edges of the near-field jet, depending on the level of water vapour in the air). This may change the gradient of the predictions in our radial temperature predictions (Figure 6), but clearly warming the prediction in the mixing region close to the edge of these predictions is not desirable as it will not improve this fit to data. CO_2 hydrates may also form. This adds an extra degree of complexity to the equation of state, and EoSs

are only now considering this complexity. Here we have presented a first order modelling solution, which still requires very complex EoS. We leave the accurate inclusion of water vapour and CO_2 hydrate formation to future EoS and future dispersion calculations.

Acknowledgements

M. Callaghan and J. Leng).

References

Ahmad, M., Bögemann-van Osch, M., Buit, L., Florisson, O., Hulsbosch-Dam, C., Spruijt, M., Davolio, F., 2013. Study of the thermohydraulics of CO_2 discharge from a high pressure reservoir. Int. J. Greenhouse Gas Control 19, 63–73.

Allason, D., Armstrong, K., Cleaver, P., Halford, A., Barnett, J., 2012. Experimental studies of the behaviour of pressurised release of carbon dioxide. In: IChemE Symposium Series No. 158, IChemE. pp. 142–152.

Brown, J., Holt, H., Helle, K., 2014a. Large Scale CO_2 Releases for Dispersion Model and Safety Study Validation. Energy Procedia 63, 2542–2546.

Brown, S., Martynov, S., Mahgerefteh, H., Fairweather, M., Woolley, R.M., Wareing, C.J., Falle, S.A.E.G., Rutters, H., Niemi, A., Zhang, Y.C., Chen, S., Bensabat, J., Shah, N., Mac Dowell, N., Proust, C., Farret, R., Economou, I.G., Tsangaris,D.M., Boulougouris, G.C., Van Wittenberghe, J., 2014b. CO_2QUEST: Techno-economic Assessment of CO_2 Quality Effect on Its Storage and Transport. Energy Procedia 63, 2622–2629.

Chen, S., Jianliang, Y., Gui, X., Zhang, Y., Yan, X., Proust, C., Hebrard, J., 2016. CO2QUEST Deliverable 2.5 Report: "Experimental studies of the atmospheric dispersion of CO_2 at a large scale and near pipeline crack". Dalian University of Technology, China; INERIS, France.

Connolly, S., Cusco, L., 2007. Hazards from high pressure carbon dioxide releases during carbon dioxide sequestration processes. In: IChemE Symposium Series No. 153, IChemE. pp. 1–5.

Cooper, R., 2012. National Grid's COOLTRANS research programme. Journal of Pipeline Engineering 11, 155–172.

Cooper, R., Barnett, J., 2014. Pipelines for transporting CO_2 in the UK. Energy Procedia 63, 2412–2431.

Demetriades, T.A., Graham, R.S., 2016. A new equation of state for CCS pipeline transport: Calibration of mixing rules for binary mixtures of CO_2 with N_2, O_2 and H_2. The Journal of Chemical Thermodynamics 93, 294–304.

Diamantonis, N.I., Boulougouris, G.C., Tsangaris, D.M., El Kadi, M.J., Saadawi, H., Nagahban, S., Economou, I.G., 2013. Thermodynamic and transport property models for carbon capture and sequestration (CCS) with emphasis on CO_2 transport. Chemical Engineering Research and Design 91, 1793–1806.

Dixon, C.M., Gant, S.E., Obiorah, C., Bilio, M., 2012. Validation of dispersion models for high pressure carbon dioxide releases, in: IChemE Symposium Series No. 158, IChemE. pp. 153–163.

Dixon, C.M., Hasson, M., 2007. Calculating the release and dispersion of gaseous, liquid and supercritical CO_2, in: IMechE Seminar on Pressure Release, Fires and Explosions, London, IMechE.

Dixon, C.M., Heynes, O., Hasson, M., 2009. Assessing the hazards associated with release and dispersion of liquid carbon dioxide on offshore platforms, in: 8th World Congress of Chemical Engineering, Montreal.

Falle, S.A.E.G., 1991. Self-similar jets. Monthly Notices of the Royal Astronomical Society 250, 581–596.

Falle, S.A.E.G., 2005. AMR applied to non-linear elastodynamics, in: Plewa, T., Linde, T., Weirs, V.G. (Eds.), Proceedings of the Chicago Workshop on Adaptive Mesh Refinement Methods, Springer Lecture Notes in Computational Science and Engineering v.41, Springer, New York U.S.A.. pp. 235–253.

Gant, S.E., Narasimhamurthy, V.D., Skjold, T., Jamois, D., Proust, C., 2014. Evaluation of multi-phase atmospheric dispersion models for application to Carbon Capture and Storage. Journal of Loss Prevention in the Process Industries 32, 286–298.

Gernert, J., Span, R., 2016. EOSCG: A Helmholtz energy mixture model for humid gases and CCS mixtures. The Journal of Chemical Thermodyanmics 93, 274–293.

Harten, A., Lax, P.D., van Leer, B., 1983. On upstream differencing and Godunov-type schemes for hyperbolic conservation laws. SIAM Review 25, 35–61.

Hill, T.A., Fackrell, J.E., Dubal, M.R., Stiff, S.M., 2011. Understanding the consequences of CO_2 leakage downstream of the capture plant. Energy Procedia 4, 2230–2237.

Hulsbosch-Dam, C.E.C., Spruijt, M.P.N., Necci, A., Cozzani, V., 2012a. As approach to carbon dioxide particle distribution in accidental releases. Chemical Engineering Transactions 26, 543–548.

Hulsbosch-Dam, C.E.C., Spruijt, M.P.N., Necci, A., Cozzani, V., 2012b. Assessment of particle size distribution in CO_2 accidental releases. J. Loss Prevention in the Process Industries 25, 254–262.

Jäger, A., Span, R., 2012. Equation of state for solid carbon dioxide based on the Gibbs free energy. J. Chem. Eng. Data. 57, 590–597.

Li, H., 2008. Thermodynamic Properties of CO_2 Mixtures and Their Applications in Advanced Power Cycles with CO_2 Capture Processes . Royal Institute of Technology, Stockholm, Sweden.

Liu, Y., Calvert, G., Hare, C., Ghadiri, M., Matsusaka, S., 2012b. Size measurement of dry ice particles produced from liquid carbon dioxide. Journal of Aerosol Science 48, 1–9.

Liu, X., Godbole, A., Lu, C., Michal, G., Venton, P., 2014. Source strength and dispersion of CO_2 releases from high-pressure pipelines: CFD model using real gas equation of state. Applied Energy 126, 56–68.

Mazzoldi, A., Hill, T., Colls, J.J., 2008a. CFD and Gaussian atmospheric dispersion models: a comparison for leak from carbon dioxide transportation and storage facilities. Atmos. Environ. 42, 8046–8054.

Mazzoldi, A., Hill, T., Colls, J.J., 2008b. CO_2 transportation for carbon capture and storage: sublimation of carbon dioxide from a dry ice bank. International Journal of Greenhouse Gas Control 2, 210–218.

Mazzoldi, A., Hill, T., Colls, J.J., 2011. Assessing the risk for CO_2 transportation within CCS projects, CFD modelling. International Journal of Greenhouse Gas Control 5, 816–825.

Peng, D.Y., Robinson, D.B., 1976. A new two-constant equation of state. Industrial and Engineering Chemistry: Fundamentals 15, 59–64.

Porter, R.T.J., Fairweather, M., Pourkashanian, M., Woolley, R.M., 2015. The range and level of impurities in CO_2 streams from different carbon capture sources. Int. J. Greenhouse Gas Control 36, 161–174.

Proust, C., Hebrard, J., Jamois, D., 2016. CO2QUEST Deliverable 2.4 Report: "Experimental investigation of the dispersion of impure CO2 in the atmosphere at a small/medium scale". L'Institut National de l'Environnement Industriel et des Risques (INERIS), Departmen PHDS, Parc Technologique ALATA, BP 2, 60550 Verneuil-en-Halatte, France.

Pursell, M., 2012. Experimental investigation of high pressure liquid CO_2 release behaviour. In: IChemE Symposium Series No. 158, IChemE. pp. 164-171.

Span, R., Wagner, W., 1996. A new equation of state for carbon dioxide covering the fluid region from the triple-point temperature to 1100 K at pressures up to 800 MPa. Journal of Physical and Chemical Reference Data 25, 1509–1596.

Span, R., Eckermann, T., Herrig, S., Hielscher, S., Jäger, A., Thol, M., 2015. TREND. Thermodynamic Reference and Engineering Data 2.0.1.. Lehrstuhl fuer Thermodynamik, Ruhr-Universitaet Bochum.

van Leer, B., 1977. Towards the ultimate conservative difference scheme. IV. A new approach to numerical convection. Journal of Computational Physics 23, 276–299.

Wareing, C., Woolley, R.M., Fairweather, M., Falle, S.A.E.G., 2013a. A composite equation of state for the modelling of sonic carbon dioxide jets in carbon capture and storage scenarios. AIChE Journal 59, 3928–3942.

Wareing, C., Fairweather, M., Peakall, J., Keevil, G., Falle, S.A.E.G., Woolley, R.M., 2013b. Numerical modelling of particle-laden sonic CO_2 jets with experimental validation, in: Zeidan, D. (Ed.), AIP Conference Proceedings of the 11th International Conference of Numerical Analysis and Applied Mathematics, AIP Publishing. pp. 98–102.

Wareing, C., Fairweather, M., Falle, S.A.E.G., Woolley, R.M., 2014a. Validation of a model of gas and dense phase CO_2 jet releases for carbon capture and storage application. Int. J. Greenhouse Gas Control 20, 254-271.

Wareing, C., Fairweather, M., Falle, S.A.E.G., Woolley, R.M., 2014b. Modelling punctures of buried high-pressure dense phase CO_2 pipelines in CCS applications. Int. J. Greenhouse Gas Control 29, 231-247.

Wareing, C., Woolley, R.M., Fairweather, M., Peakall, J., Falle, S.A.E.G., 2015b. Numerical modelling of turbulent particle-laden sonic CO_2 jets with experimental validation. Procedia Engineering 102, 1621-1629.

Wareing, C., Fairweather, M., Falle, S.A.E.G., Woolley, R.M., 2015a. Modelling ruptures of buried high-pressure dense phase CO_2 pipelines in carbon

capture and storage applications - Part I. Validation. Int. J. Greenhouse Gas Control 42, 701-711.

Wareing, C., Fairweather, M., Falle, S.A.E.G., Woolley, R.M., 2015a. Modelling ruptures of buried high-pressure dense phase CO_2 pipelines in carbon capture and storage applications - Part II. A full-scale rupture. Int. J. Greenhouse Gas Control 42, 712-728.

Wareing, C., Fairweather, M., Woolley, R.M., Falle, S.A.E.G., 2016a. Modelling particle evolution in turbulent high pressure sonic CO_2 jets, in: Proceedings of the 8th International Symposium on Turbulence, Heat and Mass Transfer, Begell House Inc., New York. pp. *in press.*

Webber, D.M., 2011. Generalising two-phase homogeneous equilibrium pipeline and jet models to the case of carbon dioxide. J. Loss Prevention in the Process Industries 24, 356–360.

Wen, J., Heidari, A., Xu, B., Jie, H., 2013. Dispersion of carbon dioxide from vertical vent and horizontal releases - a numerical study. Proceedings of the Institution of Mechanical Engineers, Part E: Journal of Process Mechanical Engineering 227, 125–139.

Wilday, A.J., McGillivray, A., Harper, P., Wardman, M., 2009. A comparison of hazard and risks for carbon dioxide and natural gas pipelines. In: IChemE Symposium Series No. 155, IChemE. pp. 392–398.

Witlox, H.W.M., Harper, M., Oke, A., 2009. Modelling of discharge and atmospheric dispersion for carbon dioxide release. J. Loss Prevention in the Process Industries 22, 795–802.

41

Witlox, H.W.M., Stene, J., Harper, M., Nilsen, S.H., 2011. Modelling of discharge and atmospheric dispersion for carbon dioxide releases including sensitivity analysis for wide range scenarios. Energy Procedia 4, 2253–2260.

Woolley, R.M., Proust, C., Fairweather, M., Falle, S.A.E.G., Hebrard, J., Jamois, D., Wareing, C.J., 2012. Experimental Measurement and RANS Modelling of Multiphase CO2 Jet Releases, in: Hanjalic, K., Nagano, Y., Borello, D. and Jakirlic, S. (Eds.), Proceedings of the 7th International Symposium on Turbulence, Heat and Mass Transfer, Begell House Inc., New York. pp. 661–664.

Woolley, R.M., Fairweather, M., Wareing, C.J., Falle, S.A.E.G., Proust, C., Hebrard, J., Jamois, D., 2013a. Experimental measurement and Reynolds-averaged Navier-Stokes modelling of the near-field structure of multi-phase CO_2 jet releases. Int. J. Greenhouse Gas Control 18, 139–149.

Woolley, R.M., Proust, C., Fairweather, M., Falle, S.A.E.G., Wareing, C.J., Hebrard, J., Jamois, D., 2013b. Measurement and RANS Modelling of Large-Scale Under-Expanded CO2 Releases for CCS Applications, in: Simos, T.E., Psihoyios, G., and Tsitouras, C. (Eds.), AIP Conference Proceedings 1558: Proceedings of the 11th International Conference of Numerical Analysis and Applied Mathematics 2013 (ICNAAM 2013), American Institute of Physics. pp. 107–111.

Woolley, R.M., Fairweather, M., Wareing, C.J., Proust, C., Hebrard, J., Jamois, D., Narasimhamurthy, V.D., Storvik, I.E., Skjold, T., Falle,

S.A.E.G., Brown, S., Mahgerefteh, H., Martynov, S., Gant, S., Tsangaris,D.M., Economou, I.G., Boulougouris, G.C., Diamantonis, N.I.., 2014a. An integrated, multi-scale modelling approach for the simulation of multiphase dispersion from accidental CO_2 pipeline releases in realistic terrain. Int. J. Greenhouse Gas Control 27, 221–238.

Woolley, R.M., Fairweather, M., Wareing, C.J., Falle, S.A.E.G., Mahgerefteh, H., Martynov, S., Brown, S., Narasimhamurthy, V.D., Storvik, I.E., Saelen, L., Skjold, T., Economou, I.G., Tsangaris,D.M., Boulougouris, G.C., Diamantonis, N.I.., Cusco, L, Wardman, M., Gant, S., Wilday, J., Zhang, Y.C., Chen, S., Proust, C., Hebrard, J., Jamois, D., 2014b. CO_2PipeHaz: Quantitative Hazard Assessment for Next Generation CO_2 Pipelines. Energy Procedia 63, 2510–2529.

Table 1: Initial conditions for the CO2PIPETRANS tests included here, reproduced from CO2PIPETRANS test descriptions.

Description	DS1 T2	DS1 T5	DS1 T11	DS2 T3	DS2 T5	DS2 T11
Pressure (barg)	155.5	157.68	82.03	147.3	148.8	80.3
Temperature (degC)	7.84	9.12	17.44	9.8	17.8	-0.2
CO_2 fraction	1.00	1.00	1.00	1.00	1.00	1.00
Condensed phase fraction	1.00	1.00	1.00	1.00	1.00	1.00
Orifice diameter (mm)	11.94	25.62	11.94	12.7	25.4	12.7
Atmospheric conditions						
Pressure (mbara)	958.2	985.4	960.2	1017	905	995
Temperature (degC)	7.5	5.8	11.6	11.2	9.0	3.6
Relative humidity (%)	96	97	94	66	91	78

Table 2: Initial conditions for the COOLTRANS test included here, reproduced from (Wareing et al., 2014a).

Description	COOLTRANS T7
Pressure (MPa)	15.00
Temperature (degC)	7.45
CO_2 fraction	1.00
Condensed phase fraction	1.00
Orifice diameter (mm)	25.4
Atmospheric conditions	
Pressure (MPa)	0.1
Temperature (degC)	7.45

Table 3: Initial conditions for the CO_2PipeHaz tests included here, reproduced from (Woolley et al., 2012, 2013a,b).

Description	HAZ T6	HAZ T7	HAZ T8	HAZ T11	HAZ T12	HAZ T1
Reservoir Pressure (bar)	95.0	85.0	77.0	83.0	77.0	69.0
Reservoir Temperature (degC)	3.0	4.0	6.0	3.0	3.0	3.5
CO_2 fraction	1.00	1.00	1.00	1.00	1.00	1.00
Condensed phase fraction	1.00	1.00	1.00	1.00	1.00	1.00
Orifice diameter (mm)	9.0	12.0	25.0	12.0	25.0	50.0
Observed flow rate ($kg\,s^{-1}$)				7.7	24.0	40.0
Atmospheric conditions						
Pressure (MPa)	0.1	0.1	0.1	0.1	0.1	0.1
Temperature (degC)	3.0	6.0	4.0	3.0	3.0	3.5
Relative humidity (%)	> 95.0	> 95.0	> 95.0	> 95.0	> 95.0	> 95.0

Table 4: Initial conditions for the HSL tests included here, reproduced from (Pursell, 2012).

Description	HSL Test C	HSL Test D
Average feed pressure (bar)	54.5	3.55
Nozzle pressure (bar)	46.9	36.7
Nozzle temperature (degC)	11.6	2.2
CO_2 fraction	1.00	1.00
Condensed phase fraction	0.86	0.84
Orifice diameter (mm)	2.0	4.0
Laboratory conditions		
Assumed pressure (MPa)	0.1	0.1
Assumed temperature (degC)	20	20

Table 5: Initial conditions for the CO2QUEST tests included here.

Description	P_{res} (bar)	T_{res} (degC)	Mixture	D_{noz} (mm)	$P_{atmos.}$ (MPa)	$T_{atmos.}$ (degC)
Pure CO_2 tests						
QUEST T12	56	16-18	100% liquid CO_2	6.0	0.1	18
QUEST T14	37	-5 - -2	100% liquid CO_2	6.0	0.1	10
DUT Trial 1	53	20	100% CO_2, two-phase	233.0	0.1	36
DUT Test 1	42-54	10-20	100% gas CO_2	50.0	0.1	1.5
Impure CO_2 tests						
QUEST T9	73	23-30	98.4% CO_2, 1.6% CH_4	6.0	0.1	26
QUEST T13	63	16	95.6% CO_2, 4.4% CH_4	6.0	0.1	18
QUEST T15	65	13	95.5% CO_2, 4.5% N_2	6.0	0.1	13
QUEST T16	57	8	95.6% CO_2, 2.2% N_2, 2.2% CH_4	6.0	0.1	11
QUEST T19	51	6	95.9% CO_2, 4.1% CH_4	6.0	0.1	9
QUEST T22	56	10	95.9% CO_2, 4.1% CH_4	12.0	0.1	14
QUEST T23	63	11	95.5% CO_2, 4.5% N_2	12.0	0.1	14
QUEST T24	57	10	96.0% CO_2, 2.1% N_2, 1.9% CH_4	12.0	0.1	10
QUEST T25	63	11	95.5% CO_2, 4.5% N_2	12.0	0.1	12

Description:	Liquid CO_2 tests	Pure CO_2	Impure CO_2
Based on:	COOLTRANS T7	QUEST T12	adapted QUEST T12
Reference:	Wareing et al. (2013b)		
Reservoir conditions			
Pressure (MPa)	15.00	5.70	5.70
Temperature (degC)	7.45	15.2	3.0
Mixture	100% liquid CO_2	100% liquid CO_2	96% CO_2, 4% N_2
Atmospheric conditions			
Pressure (MPa)	0.1	0.1	0.1
Temperature (degC)	7.45	18.0	18.0
Inlet conditions			
Diameter (mm)	24.3	6.0	6.0
Pressure (MPa)	4.14	1.469	1.498
Temperature (degC)	6.85	-29.15	-33.15
Mean velocity ($\mathrm{m\,s^{-1}}$)	105.60	136.5	135.7
Liquid fraction (kg/kg)	1.00 / 0.80 / 0.60	0.684	0.693
Density ($\mathrm{kg\,m^{-3}}$)	883.5 / 392.1 / 252.0	111.86	112.68
Mass-flow ($\mathrm{kg\,s^{-1}}$)	43.3 / 19.2 / 12.3	0.432	0.432

Table 6: Inlet conditions considered here.